SAFE: A Novel Approach to AI Weather Evaluation through Stratified Assessments of Forecasts over Earth

Anonymous authors
Paper under double-blind review

Abstract

The dominant paradigm in machine learning is to assess model performance based on average loss across all samples in some test set. This amounts to averaging performance geospatially across the Earth in weather and climate settings, failing to account for the non-uniform distribution of human development and geography. We introduce Stratified Assessments of Forecasts over Earth (SAFE), a package for elucidating the stratified performance of a set of predictions made over Earth. SAFE integrates various data domains to stratify by different attributes associated with geospatial gridpoints: territory (usually country), global subregion, income, and landcover (land or water). This allows us to examine the performance of models for each individual stratum of the different attributes (e.g., the accuracy in every individual country). To demonstrate its importance, we utilize SAFE to benchmark a zoo of state-of-the-art AI-based weather prediction models, finding that they all exhibit disparities in forecasting skill across every attribute. We use this to seed a benchmark of model forecast fairness through stratification at different lead times for various climatic variables. By moving beyond globally-averaged metrics, we for the first time ask: where do models perform best or worst, and which models are most fair? To support further work in this direction, the SAFE package is open source and available at `https://anonymous.4open.science/r/safe-E7C7`.

1 Introduction

Artificial intelligence weather prediction (AIWP) models, alternatively machine learning weather prediction (MLWP) models or neural weather models (NWM), are becoming increasingly competitive with traditional numerical weather prediction (NWP) models. All of these approaches are typically used in making medium-range weather forecasts (interchangeably, "prediction"). The range of a forecast is determined by its lead time τ. When a weather prediction model is fed the state of variables at time d, its task is to predict the state of those variables (or some subset of them) at time $d + \tau$. There is no consistent definition for medium-range, with the European Centre for Medium-Range Weather Forecasts (ECMWF) defining it as any prediction made with τ (or $n \times \tau$ if taking an autoregressive rollout of n steps) within 0–15 days (European Centre for Medium-Range Weather Forecasts, 2025b), while other sources more narrowly define it as 3–7 days (Meteorological Society; Weather Prediction Center). AIWP models are seeing increasing adoption in interfaces where they provide these medium-range forecasts, from Google's Weather app (Leffer, 2024) to various experimental models at the National Oceanic and Atmospheric Administration (NOAA) (Potvin et al., 2025; Sadeghi Tabas et al., 2025).

Root mean square error (RMSE) is the preeminent metric used in assessing the quality of AIWP models (Radford et al., 2025; Rasp et al., 2020). The general form of RMSE is

$$\sqrt{\frac{\Sigma_{y \in Y}(\hat{y} - y)^2}{|Y|}} \tag{1}$$

1

where Y is the set of all ground truth variable values that a model is trying to predict, and $\hat{y}$ is the model's prediction for each corresponding $y \in Y$. Every y is the value of some variable (e.g., temperature) at some point in time $d \in D$, longitude $i \in I$, latitude $j \in J$, and, for certain atmospheric variables, vertical level $v \in V$.

There are various approaches for how different models handle being able to make predictions at different lead times. The naive approach is to train a model with the ability to predict some fixed $\tau' \in T$ amount of time in the future, where T is a set of durations. This allows the model to forecast the weather with temporal resolution of τ' (i.e., multiples of τ' after the timestamp of the input variables) through autoregressive rollout. This is the approach taken by Keisler (Keisler, 2022), the Spherical CNN (Esteves et al., 2023), FourCastNet (Pathak et al., 2022), and the spherical Fourier neural operator (SFNO) (Bonev et al., 2023), all with $\tau' = 6$ hours. Pangu-Weather (Bi et al., 2022) trains four different models, each with a different, fixed lead time. This is used in tandem with a greedy algorithm that minimizes the number of autoregressive steps that need to be taken to make a prediction at any given lead time (which must be a multiple of their smallest lead time model). FuXi (Chen et al., 2023) uses a cascaded set of three different models that cover different ranges of lead times.

The square of RMSE, mean squared error (MSE), frequently referred to as the $L2$ loss, is often used as a training objective. This is the case for Spherical CNN (Esteves et al., 2023) and GenNet (Lopez-Gomez et al., 2023). GraphCast (Lam et al., 2023) and GenCast (Price et al., 2023) use weighted MSE loss functions. Keisler takes a weighted sum of MSE values (Keisler, 2022). NeuralGCM (Kochkov et al., 2024) has a five-term loss function, each of which is a variation of MSE. FuXi (Chen et al., 2023) uses the mean absolute error (MAE, the $L1$ counterpart of MSE).

The underlying commonality across all of these functions is that they completely reduce across the spatial dimensions I and J. A significant issue with spatial averaging for evaluation is that it becomes unknown precisely where models are and are not performing well. Accordingly, it is impossible to know whether they can be trusted at inference time in a given location. This all despite the fact that erroneously mild temperature predictions increases mortality (Shrader et al., 2023) and previous investigation which shows the existence of temperature prediction disparities in the context of the United States alone (Washington Post, 2024). With SAFE, we uncover spatial disparities in performance across the globe by separating the spatial dimensions into different strata and calculating performance within each. This enables us to understand where models perform best, and facilitates a quantitative fairness evaluation and benchmark across models. Thus, we have two main contributions:

1. The first comprehensive evaluation of fairness in AI weather prediction, demonstrating systemic spatial disparities exist.
2. The introduction of SAFE, a new open-source package that facilitates such evaluations.

> **Takeaway 1**
>
> The state of the art of AI weather prediction relies on spatially-averaged objective functions and evaluation metrics. This masks disparities that exist in where models perform well, despite the fatal consequences of poor predictive power.

2 RELATED WORK

2.1 REGION STRATIFICATION

WeatherBench 2 (WB2) (Rasp et al., 2024) is an existing benchmark that assesses the spatially-averaged error of models using weather data from ERA5, ECMWF's most modern reanalysis dataset (Hersbach et al., 2020). It provides functionality to get per-region RMSE, but these regions are coarse-grained and exclusively rectangular, making them unusable for the real-world attributes we care about. There are 20 of these regions, 3 that are hemispheric (North, Tropical, and Southern) and 17 geographic. These regions are overlapping and include oceans, but the geographic regions miss considerable sections of populated landmass (including but not limited to significant portions of Central America, Eastern Africa, Brazil, California, and the island of New Guinea). The hemispheric

regions cover the whole globe, with the Tropical region bounded by the $\pm 20°$ latitude lines. GraphCast reports per-region RMSE for T850 and Z500 in Supp. Mat. Fig. S14–S16 on these naively defined regions (Lam et al., 2023). NeuralGCM also only looks at the region attribute, considering only North Atlantic, Northeast Pacific, Northwest Pacific, Other North, South Indian, South Pacific, Other South, Tropics ($\pm 20°$), Extratropics ($[30°, 70°]$) (Kochkov et al., 2024), tropical cyclone tracks in the Atlantic, and the Intertropical Convergence Zone and atmospheric river in the Atlantic. Later, in supplementary material, Kochkov et al. (2024) redefine the tropics as ($\pm 15°$) and the extratropics as ($[25°, 55°]$).

Stable equitable error in probability space (SEEPS) (Rodwell et al., 2010) is a metric that was introduced to assess the quality of precipitation forecasts in particular. In the original paper (Rodwell et al., 2010), the authors perform region-specific analysis of forecasts in South America, Europe, and the extropics. Again, however, the region shapes are defined with crude, rectangular boundaries ([70°W–35°W, 40°S–10°N], [12.5°W–42.5°E, 35°N–75°N], and [above 30°N or below 30°S], respectively).

In contrast, the regions used within SAFE cover all landmass (including islands) across the Earth and are carefully crafted to not include oceanic landcover (i.e., they are not the crude rectangular boundaries used in existing work). This more aptly captures metrics for where fairness in weather forecasts matters most: the places where people live. Our regions are non-overlapping, except at their borders where gridpoint polygons stretch over the border (this being an artifact of finite resolution). Additionally, we include attribute categories hitherto ignored in the literature: territory, income, and landcover.

> **Takeaway 2**
>
> Existing approaches to stratify AIWP model performance are rare and at best utilize crude rectangular boundaries, operating only on the region attribute.

2.2 FAIRNESS METRICS

The standard approach to assessing fairness in continuous regression problems is to binarize the outcome based on some threshold for predicted value $\hat{y}$ (Jui & Rivas, 2024; Mehrabi et al., 2021; Barocas et al., 2023), and typically are only used in binary (two strata) settings as noted by Yan et al. (2021). This was the case with the United States' erstwhile four-fifths rule, which enforced fairness in hiring through the difference in binary outcome rates across binary group labels. There is a dearth of work and metrics that measure fairness in the continuous output space of variables as noted by Agarwal et al. (2019). Agarwal et al. (2019) attempts to address this by defining fairness metrics for continuous regression cases where the loss function is 1-Lipschitz under the ℓ_1 norm. However, with climatic variables, y, $\hat{y}$ are not bounded by $[0, 1]$ and often exceed 1 (as is the case with all the variables we explore in this work), and the loss function Equation 1 includes the exponential term $(\hat{y} - y)^2$. This means the fairness metrics of Agarwal et al. (2019) cannot apply. Other works on fairness for continuous regression utilize the difference in average $\hat{y}$ across two strata only (Suárez Ferreira et al., 2025; Fitzsimons et al., 2019; Calders et al., 2013).

In summary, fairness metrics used in both the machine learning literature and high impact legal settings are often simple differences in performance calculated with subtraction (e.g., statistical parity difference, equal opportunity difference). The greatest absolute difference and variance measurements we define in subsubsection 3.2.3 are thus firmly grounded in this existing literature. By considering more than two strata at a time, our metrics push the field further. Furthermore, the modular design of SAFE makes it easily extensible to incorporate future fairness metrics as they are developed.

3 SAFE

In this paper we create a framework for performing Stratified Assessments of Forecasts over Earth (SAFE). This tool enables stratification by various geographically-related attributes, allowing the user to see the fine-grained quality of a set of predictions when broken down by the different constituent groups, or strata, of each attribute. We leverage SAFE to benchmark the fairness of existing AIWP models.

> **Takeaway 3**
>
> We introduce SAFE, an open source python library that integrates different data sources and facilitates stratified fairness evaluations of AI weather and climate models.

3.1 DATA SOURCES

Within SAFE, we provide the ability to investigate different attributes: territory, global subregion, income, and landcover. The strata within the territory attribute is typically the country which a gridpoint is located within, though there are some sub-national or not universally recognized territories. Territory borders are pulled from the geoBoundaries Global Administrative Database (Runfola et al., 2020). Any gridpoint overlapping with any land will be classified as "land" for the landcover attribute and otherwise as "water". Global subregions follow the United Nation's classifications over territories (United Nations). The income stratum of a gridpoint is one of "high income", "upper-middle income", "lower-middle income", or "low-income" as defined by the World Bank's classification for the gridpoint's encompassing territory (World Bank); the World Bank uses the gross national income (GNI) per capita of the territory, calculated using the Atlas methodology. The polygons associated with each strata are accessed through the MIT-licensed pygeoboundaries_geolab package.[1] This package is a python wrapper for the geoBoundaries Global Administrative Database (Runfola et al., 2020), which itself is made available under a open license CC-BY 4.0.

3.2 METHODS

3.2.1 STRATIFICATION

Forecasts made over the Earth are associated with specific (longitude, latitude) coordinates, or "gridpoints" on the Earth. Each pair of coordinates is converted into the polygon that is centered on the gridpoint but which covers all the quadrilateral surface area defined by extending its borders to the midpoint with its neighbors in both the longitude and latitude directions. To unify the coordinate system across all integrated data sources, latitude ranges [-90, 90] with index 0 at -90, and longitude [-180, 180] but with index 0 at 0 and a wraparound from 180 to -180 in the middle. This is because polygons and associated attribute metadata sourced from pygeoboundaries_geolab follows this coordinate system, and it is easier to bring the other tabular data into conformance than modify this.

The forecasts for a gridpoint's polygon are associated with all of the strata that have any polygon which intersects it. While this will double count some gridpoints towards different strata, measures are taken so that no single gridpoint counts more than once within a given strata. The double counting that does occur is in line with the philosophy of SAFE, as the alternative is that—without high enough resolution—there will be strata for which no data is recorded, rendering them invisible and left out of fairness assessments. Importantly, this "double counting" is a different phenomenon from the "double penalty" described by Gilleland et al. (2009). In total, there are 231 territory, 23 subregion, 4 income, and 2 landcover strata. Of the 231 territories, 213 have an associated income strata. 76 are classified as high-income, 57 as upper-middle-income, 45 as lower-middle-income, and 34 as low-income. Subregions vary from having 1 territory (Antarctica) to 25 (Caribbean). More details on the strata are in Appendix B.

3.2.2 AREA WEIGHTING

In calculating the loss function for training it is common to weight the (squared if $L2$) difference in variable prediction and ground truth by the area of the grid cell the forecast was made at before averaging. This is the case with all six models we assess: GraphCast (Lam et al., 2023) Supp. Mat. Eq. 19, Keisler (Keisler, 2022) section 3.3.3, Pangu-Weather (Bi et al., 2022) Eq. 2, Spherical CNN—which refers to Rasp & Thuerey (2021) for training details, FuXi (Chen et al., 2023) Eq. 2, and NeuralGCM (Kochkov et al., 2024) Supp. Mat. G.4; as well as in other state-of-the-art models including but not limited to GenCast (Price et al., 2023) Supp. Mat. D.4, FGN (Alet et al., 2025) Eq. 5, and FourCastNet 3 (Bonev et al., 2025) Eq. 50. This weight varies with latitude. The reason for latitude weighting is that, when using an equiangular gridding, the gridpoints are closer together near

---

[1] https://github.com/ibhalin/pygeoboundaries

the poles than they are at the equator. This results in a higher density of samples per area at the poles, which left unaccounted for could cause the model to overfit to forecasting polar weather.

Complicating the matter, Earth is an oblate spheroid with an equatorial radius of 6,378,137m and a smaller polar radius of 6,356,752m. However, no existent python library known to the authors takes this into account to get the precise surface area of equiangular grid cells on Earth's surface. The assumption of a spherical Earth yields surface areas near the poles that are still greater than they are in reality, meaning the very problem latitude weighting aims to address persists. The standard solution would be to convert the cells to vector data and get the area of polygons. However, virtually every approach, both training/evaluating (Lam et al., 2023; Keisler, 2022; Bi et al., 2022; Kochkov et al., 2024; Pathak et al., 2022; Bonev et al., 2023; Alet et al., 2025; Bonev et al., 2025) and benchmarking (Rasp et al., 2024; Leeuwenburg et al., 2024), make the simplifying assumption of a perfectly spherical Earth. WB2 takes this approach in computing its metrics as well (Rasp et al., 2024). As part SAFE, we have provided a utility that can get the surface area of grid cells on the Earth while taking into account its oblate geometry. We use the equation for getting the surface area of oblate spheroid caps from Calvimontes (2018) Eq. 49 which builds on the model developed by Whyman & Bormashenko (2009). For testing, the total surface area of the Earth was found with the equation for oblate spheroid surface area from Beyer (1987) p. 131, yielding an approximation of $510,065,604,944,206.145m^2$. A spherical model overestimates the latitude weight (normalized by mean grid cell area) of the polar grid cells (i.e., the most northern or southern grid cells) by 0.7% with $1.5°$ resolution and by 504% with $0.25°$ resolution.

In calculating the RMSE as reported throughout this paper, we use these exact surface areas and get the weights by normalizing the grid cell areas by the mean cell area. This same normalization is used in WB2 (Rasp et al., 2024) and is common in training (Pathak et al., 2022; Bonev et al., 2023).

> **Takeaway 4**
>
> SAFE introduces a new state-of-the-art level of accuracy in latitude weighting, a normalization technique used in virtually all AI weather or climate work.

3.2.3 METRICS

Model performance metrics. The main metric utilized in SAFE is the latitude-weighted RMSE, which is averaged temporally by initialization time (the timestamp of the climate variables fed into the model) not lead time (the amount of time into the future for which to forecast the state of climate variables at), and averaged spatially within each strata. Unless otherwise specified, reported RMSE refers to this. The anomaly correlation coefficient (ACC) is another evaluation metric that is often used for cross-model comparison. It is the only scale-free metric that is commonly used for this purpose. Like RMSE, ACC is spatially averaged (European Centre for Medium-Range Weather Forecasts, 2025a) and would thus benefit from stratified assessment. The fact that the most popular metrics employ spatial averaging underscores the need for SAFE. We emphasize RMSE in this work under the same rationale as taken by WeatherBench: the similarity between RMSE and the models' training objectives (Rasp et al., 2020). Furthermore, RMSE is the predominant metric reported in the literature. In this work we focus on benchmarking deterministic models. Probabilistic, or ensemble, AIWP models have other metrics that can be used such as the continuous ranked probability score (CRPS), but also are commonly evaluated on the RMSE of the ensemble's average prediction.

We motivate the work of stratified fairness through the spatial disparities that exist in AIWP performance that is visible even on the individual gridpoint level. Figure 1 demonstrates an example of this, showing the unequal performance of GraphCast across the globe at forecasting temperature with $\tau = 72h$. The data visualized in this example can be easily accessed with SAFE through a call to the `safe_earth.metrics.errors.stratified_rmse` function.

Fairness metrics. We define two metrics for measuring fairness. Both operate on the level of data for individual variables and individual attributes. To start, the RMSE for a model's performance on the given variable is calculated for each strata within the attribute. To characterize the worst-case disparity of each model, we measure (1) the greatest absolute difference in the per-strata RMSEs. To assess the overall nature of the model, we also measure (2) the variance in per-strata RMSEs. A maximally "fair" model will have a value of 0 for both metrics, as this would mean it
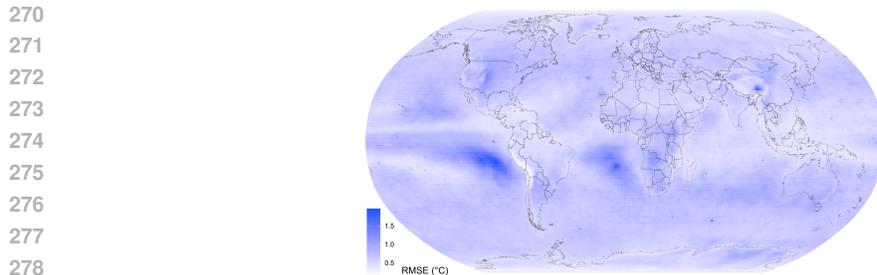
Figure 1: GraphCast displays non-uniform error in temperature prediction. The temporally-averaged gridpoint specific RMSE of temperature predictions at 850hPa (T850) made by GraphCast for every 12 hours in 2020 are shown. Predictions made with 3 day lead time, meaning they predict the temperature 72 hours after the input conditions. Lower RMSE is better. GraphCast inference predictions from WeatherBench 2, ground truth temperature values from ECMWF ERA5. Spatial resolution is 1.5 degrees.

is performing no worse on any strata than any other. These metrics are computed through calls to `safe_earth.metrics.fairness.measure_fairness` within SAFE.

> **Takeaway 5**
>
> We for the first time introduce **fine-grain stratification** in the literature. Current approaches use globally-averaged training objectives and evaluation metrics. To start, SAFE offers stratification on the attributes of territorial affiliations (country), global subregion, income, and landcover (land or water).

4 BENCHMARKING AIWP FORECAST FAIRNESS: DEMONSTRATING SAFE

To minimize computational costs, we investigate models with already available predictions. This eliminates the need for model training or inference, reducing the carbon footprint of our research. WB2 provides easily-accessible cloud datasets of ERA5 data and inference runs in the year 2020 for a number of models. Because of the unified access endpoints and resolution, we use the models available through these datasets to begin our investigation. Furthermore, these models are among the most state of the art (by standard metrics such as RMSE and ACC) (Rasp, 2024), so it is in fact preferable to study these than retrain our own, potentially inferior models.

4.1 FORECASTS ASSESSED

In this work with utilize WB2's $1.5°$ resolution equiangular predictions on ERA5. We choose the $1.5°$ resolution (240×121 in terms of longitude by latitude) because it has the most amount of models with provided forecasts at a single common resolution. The forecasts provided are made on ERA5 data from 2020. WB2 retrieved this subset of ERA5 data from ECMWF via the Copernicus Climate Data Store, which makes its products available through an open license.[2] WB2 itself is available through an Apache License 2.0.

The models evaluated are GraphCast (Lam et al., 2023), Keisler (Keisler, 2022), Pangu-Weather (Bi et al., 2022), Spherical CNN (Esteves et al., 2023), FuXi (Chen et al., 2023), and NeuralGCM (Kochkov et al., 2024); more details on these models are available in Appendix A. All of the assessed models were trained on ERA5 data, making it an appropriate common benchmark, and none of them included 2020 in their training set. The set of lead times τ that is common to the provided predictions for all models is every 12 hours up to 10 days, so we assess all models at each of these.

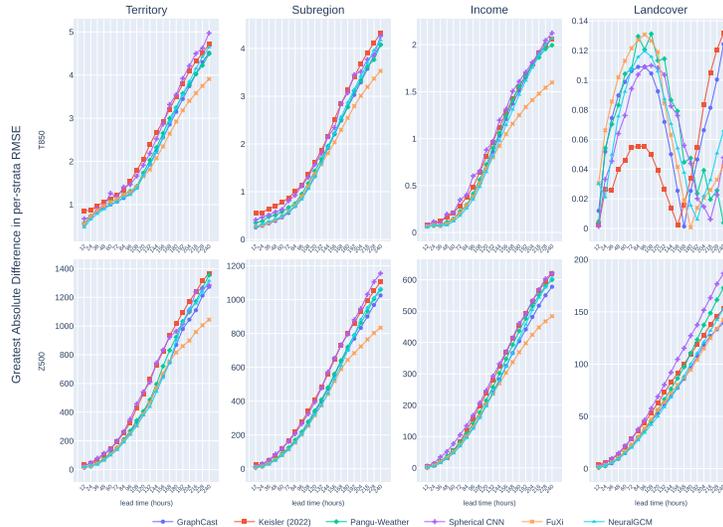[2]https://apps.ecmwf.int/datasets/licences/copernicus/

Figure 2: Greatest absolute difference of any two per-strata RMSE for each attribute when predicting T850 and Z500 at different lead times. Lower difference is more fair. Starting at a lead time of about one week, FuXi is the most fair model across all attributes and variables.

4.2 VARIABLES

In line with WeatherBench (Rasp et al., 2020; 2024), we choose as our variables y the atmospheric temperature at 850hPa ("T850", unit: K) and geopotential at 500hPa ("Z500", unit: $m^2 s^{-2}$) as benchmark variables for comparing cross-model performance in this experiment. Geopotential is the strength of Earth's gravitational field, so predicting the geopotential at a fixed atmospheric pressure level (500hPa) amounts to predicting the vertical synoptic-scale distribution of pressure in Earth's atmosphere. This knowledge is highly useful in meteorological predictions (Lam et al., 2023).

These variables are the most prevalent commonality between different model developers' assessments; that is, they are used by default in reporting model skill for their meteorological importance as outlined above. In their original papers, Pangu-Weather (Bi et al., 2022), Spherical CNN (Esteves et al., 2023), FourCastNet (Pathak et al., 2022), FuXi (Chen et al., 2023), Keisler (Keisler, 2022), and NeuralGCM (Kochkov et al., 2024) are primarily evaluated with T850 and Z500, while GraphCast is an outlier (Lam et al., 2023) reporting mainly on just Z500. We provide results on other variables of interest in Appendix E; those experiments find the same results of systemic bias.

4.3 EXPERIMENTAL DESIGN

The main data we collect in our experiments involves taking the area-weighted squared difference between the models prediction $\hat{y}$ and the ERA5 ground truth value y at every individual gridpoint, for every lead time $\tau \in \{12h, 24h, ..., 240h\}$, at every 12 hour interval in 2020.

Then, for each of our four attributes and both variables, we calculate the per-strata RMSE (averaged temporally over the year) at all 20 lead times by taking the RMSE when spatially averaging over only the gridpoints within that strata. This allows us to see which stratum the models are performing best or worst within.

Lastly, for each attribute and variable, we take the greatest absolute difference in per-strata RMSE of any pair of per-strata RMSE with the same attribute and variable. We also take the variance of all the per-strata RMSE to characterize the spread of model performance. This allows us to quantify the fairness of a model's predictions, where the smaller the difference and variance are, the more fair the model. As perfectly fair models are defined as having values of 0 for the metrics we define, the greater these metrics are the more biased a model is considered.
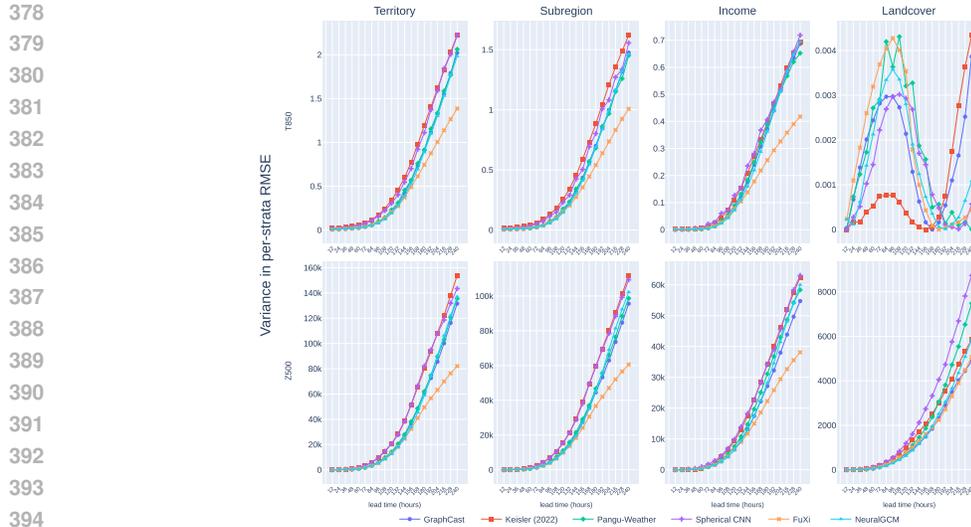
Figure 3: Variance of all the per-strata RMSE for each attribute when predicting T850 and Z500 at different lead times. Lower variance is more fair.

4.4 RESULTS

General fairness. As seen in Figure 2, the fairness of predictions begin to rapidly decline once the lead time surpasses three days; that is, the greatest absolute difference in RMSE of any two strata rapidly increases. Across all four attributes and all lead times, Spherical CNN and Keisler are generally the least fair. From a lead time of about a week onwards, FuXi is drastically more fair than every other model across all attributes. At early lead times, NeuralGCM appears to perform most fairly.

It is generally seen across all models and variables that the biases in predictions increase exponentially after lead time surpasses a few days. The exception appears to be a dip in bias in the landcover attribute on T850 with roughly eight days of lead time. However, the landcover attribute is a special case where it can be argued that one should care about absolute performance on the land attribute rather than inter-strata fairness. That is, we may want a pro-land bias. This dip corresponds with model's temperature predictions switching from better over land to worse over land than water (Figure 5).

We provide comprehensive benchmarks of the model fairness results in Appendix D. We also calculate the variance in per-strata RMSEs (Figure 3) which displays similar patterns as seen in the greatest absolute difference (Figure 2). The main difference with variance is that it takes a larger lead time for unfairness to start exponentially increasing. Appendix C proves the discovered biases are not driven by outliers. In Appendix E we conduct the same general fairness analysis on additional climatic variables: precipitation (6hr and 24hr cumulative), 2m temperature, and wind speed (U and V components at 10m).

Income attribute. To qualitatively characterize the growing unfairness observed in Figure 2, we take a detailed look at the income attribute. Because it only has four strata, it is easy to visualize and meaningful to explore. For lead time $\tau = 12$ hours, Keisler, Pangu-Weather, Spherical CNN, and NeuralGCM perform worst at predicting both variables in low-income territories (Figure 14).[3] However, by $\tau = 48$ hours, every model displays the trend for both variables where prediction skill decreases as income increases; this disparity continues to grow with lead time (Figure 4). This is an interesting result, and it shows that lead time is an important dimension to consider, because the disparity observed at one fixed lead time may not hold at another.

---

[3]The exception being NeuralGCM, where the per-strata RMSE on Z500 for lower-middle-income is 30.60187 versus low-income's 30.58936.
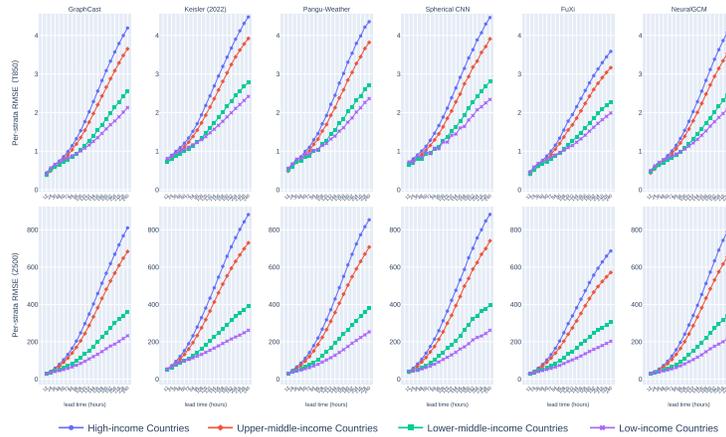
Figure 4: Per-strata RMSE for the income attribute of each model. This captures how well models perform at predicting each climatic variable stratified by the income classification for the associated country. We see that a bias against high income countries grows over time.
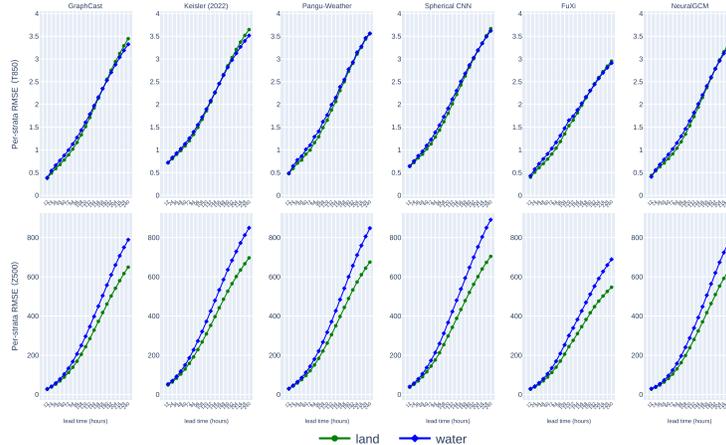

Figure 5: Per-strata RMSE for the landcover attribute of each model. This captures how well models perform at predicting each climatic variable stratified by the prediction being over land or water (oceans, seas, and many large lakes).

Landcover attribute. We also take a close look at the landcover attribute. Generally, models perform better over land than water. This can be seen in Figure 5. However, by a lead time of 9 days ($\tau = 216$ hours), all of the models except Pangu-Weather become worse at predicting temperature over land than water. In looking at greatest absolute difference and variance in RMSE, Pangu-Weather did not appear as the most fair with regards to landcover. However, we consider landcover to be a unique attribute. We have a special interest in absolute performance on the land stratum alone as that is where people live (small island nations are dutifully included in "land").[4] In this sense, Pangu-Weather behaves as we may hope in always performing better over land than water, perhaps even more so than if it had equal performance across the strata. This is an exception to the fairness paradigm we laid out before, though it is sensible as all of the other attributes' strata are subsets of the "land" strata. In those cases, we want all the strata to be treated equally. Looking at the landcover attribute as a whole, FuXi is still the most overall fair as at given lead times it has the lowest error for the land stratum.

---

[4]One exception is boats out at sea. For this case, SAFE still provides state of the art advancements as model users can now look at model performance specifically on the oceanic gridpoints they will be traveling across.

> **Takeaway 6**
>
> An example analysis made possible through SAFE **proves the existence of systemic bias in AI weather prediction** by location (at both territory and region resolution), income, and landcover for all climatic variables assessed. The bias increases with lead time.

5 FUTURE WORK

An important future direction of work on improving SAFE is incorporating more attributes. Moving beyond binary landcover, work with implicit neural representation (INR) models has shown that it is important to further consider coastlines and islands as their own strata as well (Cai & Balestriero, 2025). Additionally, population density will be added to SAFE as an attribute to better understand the degree to which different AIWP models can be a trusted decision-making tools across different human settlements. This can be done with the LandScan Global dataset (Dobson et al., 2000; Lebakula et al., 2025), and will improve on the already state-of-the-art territory-level precision of this work.

Currently, SAFE operates at inference time. It may prove beneficial to integrate tracking of fairness metrics into the training regimes of models to understand how different training dynamics affect fairness. Further, incorporating spatial stratification into training objectives could ameliorate bias. In general, investigating the underlying causes for why different models are more or less fair and how to remedy this are consequential research questions that are first raised by our work.

6 DISCUSSION

Organizations like the NOAA are beginning to incorporate ML systems in their work, citing improvements in models such as ECMWF's very own Artificial Intelligence/Integrated Forecasting System (AIFS) (Konkel, 2024). As AIWP models become increasingly relied upon, the results of this work necessitates more careful attention being paid to the stratified performance and fairness of models. By using SAFE to investigate the territory attribute, one is able to find whether a given AIWP is appropriate to leverage in decision making within that territory. This is an important discovery given the life and death consequences that forecasts can impart. The benchmark provided in this work is a first step in this direction. Moreover, SAFE empowers deployers to select the model which is most performant for their local application given the biases we prove exist. The visibility provided by SAFE into stratified forecast fairness brings this research area to light.

7 CONCLUSION

In this work we created SAFE, a python package that allows the user to assess a set of machine learning predictions made over Earth in terms of stratified fairness. Strata are available for four attributes a gridpoint may have: territorial affiliation, global subregion, gross national income per capita, and landcover. This provides developers and decision-makers alike with an important tool to break free from the default approach of spatial averaging. We apply SAFE to a set of state of the art AIWP models, finding that they all display unfair spatial disparities in performance on all four attributes. These disparities generally increase with lead time, particularly after three days. These findings justify our approach of capturing more geographically fine-tuned errors, discouraging the current reliance on spatially-averaged RMSE for characterizing AIWP models. This is an advancement upon the foundation of all AI weather and climate work.

REPRODUCIBILITY STATEMENT

We have made SAFE open source, including code for reproducing the specific results of section 4, as well as the entire generic framework for promoting similar stratified evaluations on more models and datasets. Code for generating the figures of this work is also included in the repo. We have stylistically altered them in a vector graphics editor, but the data values and representation are the same as those output by the scripts in `demos/` directory. We clearly state the origin of our climate and attribute data in the main text of the paper in subsection 3.1 and subsection 4.1; we also go into

further detail in Appendix B. The code for generating all of the data is part of the SAFE repo in `src/safe_earth/data/`. In subsubsection 3.2.3, we provide code snippets for calculating the metrics we report on.

REFERENCES

Alekh Agarwal, Miroslav Dudík, and Zhiwei Steven Wu. Fair regression: Quantitative definitions and reduction-based algorithms. In *International conference on machine learning*, pp. 120–129. PMLR, 2019.

Ferran Alet, Ilan Price, Andrew El-Kadi, Dominic Masters, Stratis Markou, Tom R. Andersson, Jacklynn Stott, Remi Lam, Matthew Willson, Alvaro Sanchez-Gonzalez, and Peter Battaglia. Skillful joint probabilistic weather forecasting from marginals, 2025. URL https://arxiv.org/abs/2506.10772.

Solon Barocas, Moritz Hardt, and Arvind Narayanan. *Fairness and Machine Learning: Limitations and Opportunities*. MIT Press, 2023.

William H Beyer. *Handbook of Mathematical Science*. CRC press, 6th edition, 1987.

Kaifeng Bi, Lingxi Xie, Hengheng Zhang, Xin Chen, Xiaotao Gu, and Qi Tian. Pangu-weather: A 3d high-resolution model for fast and accurate global weather forecast. *arXiv preprint arXiv:2211.02556*, 2022.

Boris Bonev, Thorsten Kurth, Christian Hundt, Jaideep Pathak, Maximilian Baust, Karthik Kashinath, and Anima Anandkumar. Spherical fourier neural operators: Learning stable dynamics on the sphere. In *International conference on machine learning*, pp. 2806–2823. PMLR, 2023.

Boris Bonev, Thorsten Kurth, Ankur Mahesh, Mauro Bisson, Jean Kossaifi, Karthik Kashinath, Anima Anandkumar, William D. Collins, Michael S. Pritchard, and Alexander Keller. Fourcastnet 3: A geometric approach to probabilistic machine-learning weather forecasting at scale, 2025. URL https://arxiv.org/abs/2507.12144.

Markus M Breunig, Hans-Peter Kriegel, Raymond T Ng, and Jörg Sander. Lof: identifying density-based local outliers. In *Proceedings of the 2000 ACM SIGMOD international conference on Management of data*, pp. 93–104, 2000.

Daniel Cai and Randall Balestriero. No location left behind: Measuring and improving the fairness of implicit representations for earth data. In Y. Yue, A. Garg, N. Peng, F. Sha, and R. Yu (eds.), *International Conference on Representation Learning*, volume 2025, pp. 59288–59314, 2025. URL https://proceedings.iclr.cc/paper_files/paper/2025/file/94a98f4338b6e5fba81344f961bac8e5-Paper-Conference.pdf.

Toon Calders, Asim Karim, Faisal Kamiran, Wasif Ali, and Xiangliang Zhang. Controlling attribute effect in linear regression. In *2013 IEEE 13th international conference on data mining*, pp. 71–80. IEEE, 2013.

Alfredo Calvimontes. The measurement of the surface energy of solids by sessile drop accelerometry. *Microgravity Science and Technology*, 30:277–293, 2018.

Lei Chen, Xiaohui Zhong, Feng Zhang, Yuan Cheng, Yinghui Xu, Yuan Qi, and Hao Li. Fuxi: A cascade machine learning forecasting system for 15-day global weather forecast. *npj climate and atmospheric science*, 6(1):190, 2023.

Jerome E Dobson, Edward A Bright, Phillip R Coleman, Richard C Durfee, and Brian A Worley. Landscan: a global population database for estimating populations at risk. *Photogrammetric engineering and remote sensing*, 66(7):849–857, 2000.

Carlos Esteves, Jean-Jacques Slotine, and Ameesh Makadia. Scaling spherical CNNs. In Andreas Krause, Emma Brunskill, Kyunghyun Cho, Barbara Engelhardt, Sivan Sabato, and Jonathan Scarlett (eds.), *Proceedings of the 40th International Conference on Machine Learning*, volume 202 of *Proceedings of Machine Learning Research*, pp. 9396–9411. PMLR, 23–29 Jul 2023. URL https://proceedings.mlr.press/v202/esteves23a.html.

European Centre for Medium-Range Weather Forecasts. Section 12.a statistical concepts: Deterministic data — forecast user guide, 2025a. URL `https://confluence.ecmwf.int/display/FUG/Section+12.A+Statistical+Concepts+-+Deterministic+Data#Section12.AStatisticalConceptsDeterministicData-MeasureofSkill-theAnomalyCorrelationCoefficient(ACC)`.

European Centre for Medium-Range Weather Forecasts. Medium-range forecasts, 2025b. URL `https://www.ecmwf.int/en/forecasts/documentation-and-support/medium-range-forecasts`.

Jack Fitzsimons, AbdulRahman Al Ali, Michael Osborne, and Stephen Roberts. A general framework for fair regression. *Entropy*, 21(8), 2019. ISSN 1099-4300. doi: 10.3390/e21080741. URL `https://www.mdpi.com/1099-4300/21/8/741`.

Eric Gilleland, David Ahijevych, Barbara G. Brown, Barbara Casati, and Elizabeth E. Ebert. Intercomparison of Spatial Forecast Verification Methods. *Weather and Forecasting*, 24(5):1416–1430, October 2009. ISSN 1520-0434, 0882-8156. doi: 10.1175/2009WAF2222269.1. Publisher: American Meteorological Society Section: Weather and Forecasting.

Hans Hersbach, Bill Bell, Paul Berrisford, Shoji Hirahara, András Horányi, Joaquín Muñoz-Sabater, Julien Nicolas, Carole Peubey, Raluca Radu, Dinand Schepers, et al. The era5 global reanalysis. *Quarterly journal of the royal meteorological society*, 146(730):1999–2049, 2020.

Mia Hubert and Stephan Van der Veeken. Outlier detection for skewed data. *Journal of Chemometrics: A Journal of the Chemometrics Society*, 22(3-4):235–246, 2008.

Mia Hubert and Ellen Vandervieren. An adjusted boxplot for skewed distributions. *Computational statistics & data analysis*, 52(12):5186–5201, 2008.

Tonni Das Jui and Pablo Rivas. Fairness issues, current approaches, and challenges in machine learning models. *International Journal of Machine Learning and Cybernetics*, 15(8):3095–3125, 2024.

Ryan Keisler. Forecasting global weather with graph neural networks. *arXiv preprint arXiv:2202.07575*, 2022.

Dmitrii Kochkov, Janni Yuval, Ian Langmore, Peter Norgaard, Jamie Smith, Griffin Mooers, Milan Klöwer, James Lottes, Stephan Rasp, Peter Düben, Sam Hatfield, Peter Battaglia, Alvaro Sanchez-Gonzalez, Matthew Willson, Michael P. Brenner, and Stephan Hoyer. Neural general circulation models for weather and climate. *Nature*, 632(8027):1060–1066, August 2024. ISSN 0028-0836, 1476-4687. doi: 10.1038/s41586-024-07744-y. URL `https://www.nature.com/articles/s41586-024-07744-y`.

Frank Konkel. Cloud and ai are 'fundamentally changing' ability to forecast weather, noaa chief says, 2024. URL `https://www.nextgov.com/digital-government/2024/12/cloud-and-ai-are-fundamentally-changing-ability-forecast-weather-noaa-chief-says/401453/`.

Remi Lam, Alvaro Sanchez-Gonzalez, Matthew Willson, Peter Wirnsberger, Meire Fortunato, Ferran Alet, Suman Ravuri, Timo Ewalds, Zach Eaton-Rosen, Weihua Hu, et al. Learning skillful medium-range global weather forecasting. *Science*, 382(6677):1416–1421, 2023.

Viswadeep Lebakula, Jack Gonzales, Clinton Stipek, Eve Tsybina, Andrew Zimmer, Nivedita Nukavarapu, Byeonghwa Jeong, Brandyn Reynolds, Jason Kaufman, Junchuan Fan, Aubre Martin, Whitson Buck, Scott Basford, Abbie Faxon, Shannon Meade, and Marie Urban. Landscan global 2024, October 2025. URL `https://www.osti.gov/biblio/2587445`.

Tennessee Leeuwenburg, Nicholas Loveday, Elizabeth E. Ebert, Harrison Cook, Mohammadreza Khanarmuei, Robert J. Taggart, Nikeeth Ramanathan, Maree Carroll, Stephanie Chong, Aidan Griffiths, and John Sharples. scores: A Python package for verifying and evaluating models and predictions with xarray. *Journal of Open Source Software*, 9(99):6889, July 2024. doi: 10.21105/joss.06889. URL `https://joss.theoj.org/papers/10.21105/joss.06889`.

Lauren Leffer. Ai weather forecasting can't replace humans—yet, 2024. URL `https://www.scientificamerican.com/article/ai-weather-forecasting-cant-replace-humans-yet/`.

Ze Liu, Han Hu, Yutong Lin, Zhuliang Yao, Zhenda Xie, Yixuan Wei, Jia Ning, Yue Cao, Zheng Zhang, Li Dong, et al. Swin transformer v2: Scaling up capacity and resolution. In *Proceedings of the IEEE/CVF conference on computer vision and pattern recognition*, pp. 12009–12019, 2022.

Ignacio Lopez-Gomez, Amy McGovern, Shreya Agrawal, and Jason Hickey. Global extreme heat forecasting using neural weather models. *Artificial Intelligence for the Earth Systems*, 2(1): e220035, 2023.

Ninareh Mehrabi, Fred Morstatter, Nripsuta Saxena, Kristina Lerman, and Aram Galstyan. A survey on bias and fairness in machine learning. *ACM computing surveys (CSUR)*, 54(6):1–35, 2021.

American Meteorological Society. Glossary of meteorology. URL `https://glossary.ametsoc.org/wiki/Medium-range_forecast`.

Jaideep Pathak, Shashank Subramanian, Peter Harrington, Sanjeev Raja, Ashesh Chattopadhyay, Morteza Mardani, Thorsten Kurth, David Hall, Zongyi Li, Kamyar Azizzadenesheli, et al. Fourcastnet: A global data-driven high-resolution weather model using adaptive fourier neural operators. *arXiv preprint arXiv:2202.11214*, 2022.

Corey Potvin, Montgomery Flora, Adam Clark, Patrick Burke, and Lou Wicker. Wofscast: A graphcast-based emulator for the warn-on-forecast system, 2025. URL `https://epic.noaa.gov/wofscast-a-graphcast-based-emulator-for-the-warn-on-forecast-system/`.

Ilan Price, Alvaro Sanchez-Gonzalez, Ferran Alet, Tom R Andersson, Andrew El-Kadi, Dominic Masters, Timo Ewalds, Jacklynn Stott, Shakir Mohamed, Peter Battaglia, et al. Gencast: Diffusion-based ensemble forecasting for medium-range weather. *arXiv preprint arXiv:2312.15796*, 2023.

Jacob T Radford, Imme Ebert-Uphoff, and Jebb Q Stewart. A comparison of ai weather prediction and numerical weather prediction models for 1–7-day precipitation forecasts. *Weather and Forecasting*, 40(4):561–575, 2025.

Stephan Rasp. Ai-weather sota vs time, 2024. URL `https://doi.org/10.6084/m9.figshare.28083515.v1`.

Stephan Rasp and Nils Thuerey. Data-driven medium-range weather prediction with a resnet pretrained on climate simulations: A new model for weatherbench. *Journal of Advances in Modeling Earth Systems*, 13(2):e2020MS002405, 2021.

Stephan Rasp, Peter D Dueben, Sebastian Scher, Jonathan A Weyn, Soukayna Mouatadid, and Nils Thuerey. Weatherbench: a benchmark data set for data-driven weather forecasting. *Journal of Advances in Modeling Earth Systems*, 12(11):e2020MS002203, 2020.

Stephan Rasp, Stephan Hoyer, Alexander Merose, Ian Langmore, Peter Battaglia, Tyler Russell, Alvaro Sanchez-Gonzalez, Vivian Yang, Rob Carver, Shreya Agrawal, et al. Weatherbench 2: A benchmark for the next generation of data-driven global weather models. *Journal of Advances in Modeling Earth Systems*, 16(6):e2023MS004019, 2024.

Mark J Rodwell, David S Richardson, Tim D Hewson, and Thomas Haiden. A new equitable score suitable for verifying precipitation in numerical weather prediction. *Quarterly Journal of the Royal Meteorological Society*, 136(650):1344–1363, 2010.

Olaf Ronneberger, Philipp Fischer, and Thomas Brox. U-net: Convolutional networks for biomedical image segmentation. In *Medical image computing and computer-assisted intervention–MICCAI 2015: 18th international conference, Munich, Germany, October 5-9, 2015, proceedings, part III 18*, pp. 234–241. Springer, 2015.

Daniel Runfola, Austin Anderson, Heather Baier, Matt Crittenden, Elizabeth Dowker, Sydney Fuhrig, Seth Goodman, Grace Grimsley, Rachel Layko, Graham Melville, Maddy Mulder, Rachel Oberman, Joshua Panganiban, Andrew Peck, Leigh Seitz, Sylvia Shea, Hannah Slevin, and Lauren Yougerman, Rebecca Hobbs. geoboundaries: A global database of political administrative boundaries. *PloS one*, 15(4):e0231866, 2020.

Sadegh Sadeghi Tabas, Jun Wang, Wei Lei, Mallory Row, Zhan Zhang, Lin Zhu, Jiayi Peng, and Jacob R Carley. Gfs-powered machine learning weather prediction: A comparative study on training graphcast with noaa's gdas data for global weather forecasts. *NOAA NCEP Office Note*, 2025. doi: 10.25923/xd3y-wy31.

Jeffrey G. Shrader, Laura Bakkensen, and Derek Lemoine. "Fatal Errors: The Mortality Value of Accurate Weather Forecasts", June 2023. URL https://www.nber.org/papers/w31361.

Juliett Suárez Ferreira, Marija Slavkovik, and Jorge Casillas. General procedure to measure fairness in regression problems. *International Journal of Data Science and Analytics*, pp. 1–20, 2025.

Dongdong Tian, Wei Ji Leong, Yvonne Fröhlich, Michael Grund, William Schlitzer, Max Jones, Liam Toney, Jiayuan Yao, Jing-Hui Tong, Yohai Magen, Kathryn Materna, Andre Belem, Tyler Newton, Abhishek Anant, Malte Ziebarth, Jamie Quinn, Leonardo Uieda, and Paul Wessel. PyGMT: A Python interface for the Generic Mapping Tools, October 2025. URL https://doi.org/10.5281/zenodo.17156962.

United Nations. Statistics Division, Department of Economic and Social Affairs, United Nations. standard country or area codes for statistical use. Series M, No. 49. Revision 4. 1999. URL https://unstats.un.org/unsd/publication/SeriesM/Series_M49_Rev4(1999)_en.pdf.

Washington Post. "We mapped weather forecast accuracy across the U.S. Look up your city", 2024. URL https://www.washingtonpost.com/climate-environment/interactive/2024/how-accurate-is-the-weather-forecast/.

Weather Prediction Center. Wpc medium range forecasts (days 3-7). URL https://www.wpc.ncep.noaa.gov/medr/medr.shtml.

Paul Wessel, Joaquim Freire Luis, L al Uieda, Remko Scharroo, Florian Wobbe, Walter HF Smith, and Dongdong Tian. The generic mapping tools version 6. *Geochemistry, Geophysics, Geosystems*, 20(11):5556–5564, 2019.

Gene Whyman and Edward Bormashenko. Oblate spheroid model for calculation of the shape and contact angles of heavy droplets. *Journal of Colloid and Interface Science*, 331(1):174–177, 2009.

The World Bank. World bank country and lending groups. URL https://datahelpdesk.worldbank.org/knowledgebase/articles/906519-world-bank-country-and-lending-groups.

Shen Yan, Hsien-Te Kao, Kristina Lerman, Shrikanth Narayanan, and Emilio Ferrara. Mitigating the bias of heterogeneous human behavior in affective computing. In *2021 9th International Conference on Affective Computing and Intelligent Interaction (ACII)*, pp. 1–8. IEEE, 2021.

A MODEL DETAILS

Original papers, architecture type, and number of parameters (if reported in the original paper) are described in Table 1 for all of the models we asses in our demonstration of SAFE in section 4.

B ATTRIBUTE STRATA DETAILS

Interactive maps showing the geographic locations of each strata for the different attributes is available at <URL REDACTED FOR ANONYMINITY>.

Table 1: Models assessed

Model	Architecture	Parameters
GraphCast (Lam et al., 2023)	Graph neural network (GNN)	36.7 M
Keisler (Keisler, 2022)	GNN	6.7 M
Pangu-Weather (Bi et al., 2022)	Earth-specific transformer	256 M
Spherical CNN (Esteves et al., 2023)	Spherical convolutional neural network (CNN)	Not reported
FuXi (Chen et al., 2023)	SwinV2 (Liu et al., 2022) transformer blocks in U-net (Ronneberger et al., 2015) arrangement	Not reported
NeuralGCM (Kochkov et al., 2024)	Multi-layer perceptrons (MLP) + CNNs + numerical solver	31.1 M

B.1 SUBREGIONS

The 23 strata included in the global subregion attribute are: Antarctica, Australia/New Zealand, Caribbean, Central America, Central Asia, Eastern Africa, Eastern Asia, Eastern Europe, Melanesia, Micronesia, Middle Africa, Northern Africa, Northern America, Northern Europe, Polynesia, South America, South-Eastern Asia, Southern Africa, Southern Asia, Southern Europe, Western Africa, Western Asia, and Western Europe.

B.2 INCOME

The 18 territory strata without income classifications by the World Bank are: Anguilla; Antarctica; Bonaire, Sint Eustatius, and Saba; Saint Barthelemy; Cook Islands; Falkland Islands; Guadeloupe; French Guiana; Montserrat; Martinique; Mayotte; Niue; Pitcairn Island; Réunion; Saint Helena, Ascension, and Tristan da Cunha; Vatican City; Wallis and Futuna; and Tokelau.

B.3 LANDCOVER

Due to idiosyncrasies in geoBoundaries, the landcover strata of "land" includes most lakes. Of the 15 largest by surface area, the following are included in "land": Lake Baikal, Great Bear Lake, Great Slave Lake, Lake Winnipeg, Lake Ladoga, and Lake Balkhash. Disambiguation will be improved through the integration of data sources more targeted for landcover. Datasets such as the Generic Mapping Tools (GMT) (Wessel et al., 2019), available in Python with PyGMT (Tian et al., 2025), can provide gridpoint strata of ocean, landmass, lake, land within lake, and lake within land within lake.

C ACCOUNTING FOR OUTLIERS

For each model we have assessed, the greatest absolute difference and variance in RMSE for each variable decreases as the number of stratum for the attribute decreases. This raises the question of whether the unfairness phenomenon observed results from rare outliers that appear as the geographic area of the smallest stratum decreases. To account for this, we reconduct our general fairness analysis after filtering out the set of outlier per-strata RMSE for every attribute. Because the data is skewed, we do not use Tukey's fences as a determination of outlyingness. Furthermore, as the data is bimodal at high lead times for the territory and subregion attributes, we cannot use the adjusted boxplot (Hubert & Vandervieren, 2008) or adjusted outlyingness (AO) (Hubert & Van der Veeken, 2008) methods either. Thus, we turn to local outlier factor (LOF) (Breunig et al., 2000) as our method of outlier detection. We use the default scikit-learn parameters.

Figure 6 and Figure 7 are the same as Figure 2 and Figure 3, respectively, except the outliers have been filtered out. Because the landcover attribute only has two strata, the notion of an outlier does not make sense and so this attribute has been excluded. To more easily compare the results when both including and excluding outliers, we graph the largest per-strata RMSE as a percent of the smallest per-strata RMSE in Figure 8. While there are slight differences in the greatest absolute difference in RMSE for the territory attribute (as evidenced by the different percentages), the general shape of the curves as a function of lead time holds with minor decreases in amplitude. This shows there are deeper trends in unfairness that are not being driven by outliers alone.
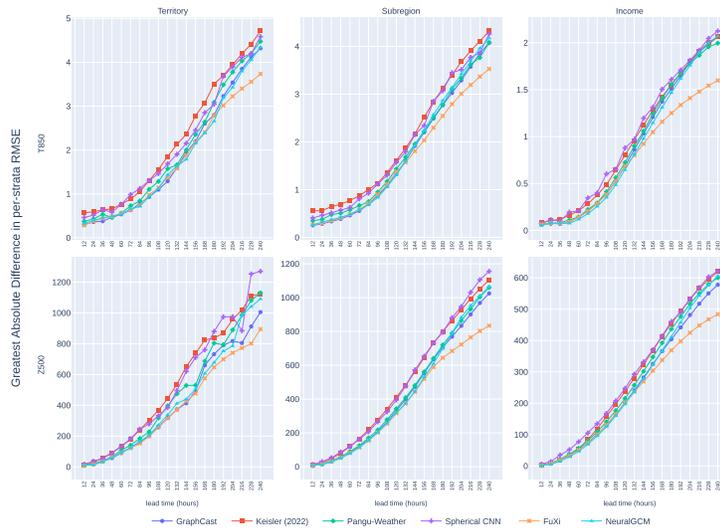
Figure 6: Greatest absolute difference of any two per-strata RMSE for each attribute when predicting T850 and Z500 at different lead times. Lower difference is more fair. Outlier RMSE values have been removed. Starting at a lead time of one week, FuXi is still the most fair model across all attributes and variables.

Figure 7: Variance of all the per-strata RMSE for each attribute when predicting T850 and Z500 at different lead times. Lower variance is more fair. Outlier RMSE values have been removed. Starting at a lead time of one week, FuXi is still the most fair model across all attributes and variables.
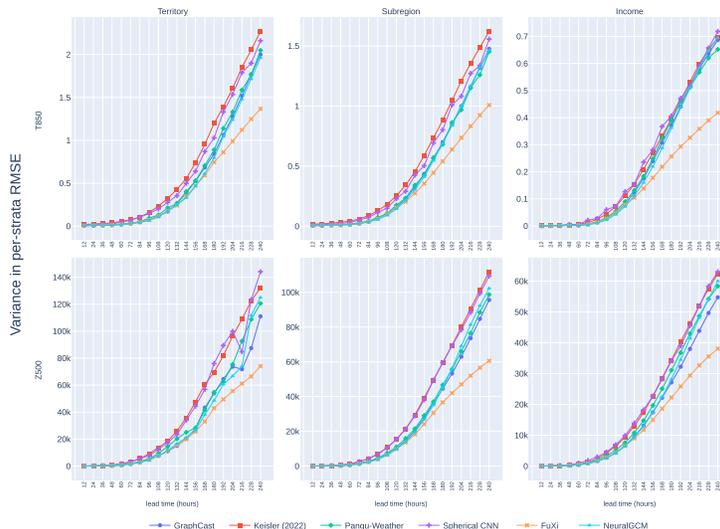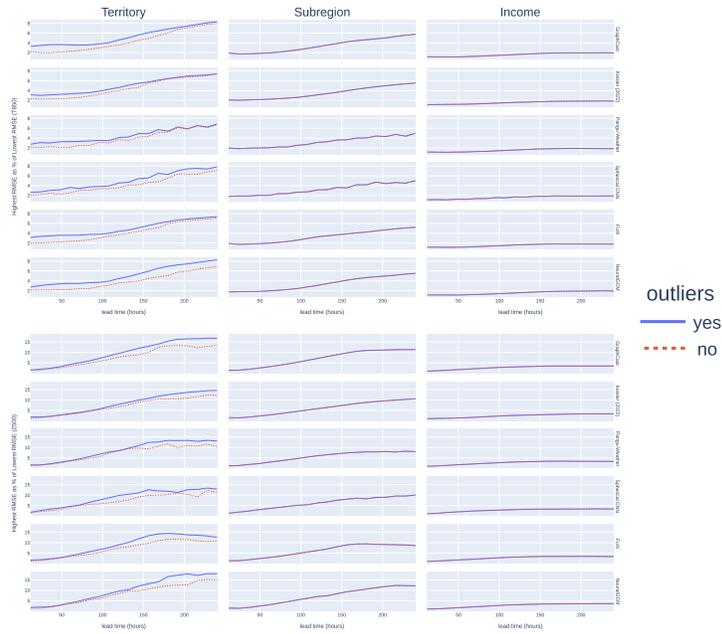
Figure 8: Highest per-strata RMSE as a percent of the lowest per-strata RMSE with and without RMSE outliers filtered out.

D FAIRNESS BENCHMARKS

Table 2: Greatest absolute difference in per-strata RMSE for territory. Lower is more fair; most fair for each variable and lead time is bolded.

Variable	Lead time (h)	Model					
		GraphCast	Keisler	Pangu-Weather	Spherical CNN	FuXi	NeuralGCM
T850	12h	0.5301	0.8523	0.5677	0.6726	0.5548	**0.4715**
T850	24h	0.7129	0.8712	0.7346	0.7011	0.7321	**0.6562**
T850	36h	0.8428	0.9704	0.8578	0.9009	0.8646	**0.7861**
T850	48h	0.9265	1.0467	0.9562	0.9670	0.9731	**0.8921**
T850	60h	0.9991	1.1356	1.0671	1.2620	1.0586	**0.9915**
T850	72h	1.0666	1.2268	1.1138	1.1681	1.1301	**1.0552**
T850	84h	**1.1528**	1.3355	1.2301	1.4047	1.2289	1.1660
T850	96h	1.2629	1.5298	1.3096	1.4621	1.2870	**1.2227**
T850	108h	1.3920	1.7896	1.4194	1.6604	1.4135	**1.3685**
T850	120h	1.6689	2.0537	1.7343	1.9129	**1.6558**	1.6819
T850	132h	1.9286	2.3906	2.0301	2.1865	**1.8117**	1.9187
T850	144h	2.2473	2.6782	2.3223	2.5244	**2.0726**	2.1994
T850	156h	2.5549	2.9147	2.6536	2.8648	**2.3466**	2.5437
T850	168h	2.8560	3.2085	2.9975	3.3171	**2.6423**	2.9141
T850	180h	3.1494	3.5049	3.2451	3.5449	**2.9232**	3.2373
T850	192h	3.4473	3.7977	3.5734	3.9219	**3.1848**	3.5434
T850	204h	3.7448	4.0875	3.7818	4.2116	**3.4015**	3.8543
T850	216h	4.0216	4.3177	4.0281	4.4993	**3.5835**	4.1497
T850	228h	4.2999	4.5044	4.2233	4.6229	**3.7494**	4.4231
T850	240h	4.5130	4.7116	4.4912	4.9728	**3.9086**	4.6413
Z500	12h	**13.4222**	31.7980	17.1554	23.3231	15.6101	17.7155
Z500	24h	25.4911	39.2029	**22.7217**	48.5697	25.4045	27.7922
Z500	36h	44.5530	63.3959	44.6666	78.6476	41.8652	**35.5452**
Z500	48h	73.7853	101.7007	74.2397	112.7660	67.0475	**63.8041**
Z500	60h	114.5105	144.6675	112.3888	143.2511	104.6706	**98.8060**
Z500	72h	149.7483	192.5330	150.8271	199.7432	150.0260	**136.3233**
Z500	84h	197.7661	254.1886	209.0000	263.5604	199.1568	**189.1055**
Z500	96h	258.1191	326.9143	268.7369	350.5695	251.8137	**243.2503**
Z500	108h	327.6491	430.2865	341.8734	457.4359	**305.2133**	305.4085
Z500	120h	396.9567	528.5107	405.2052	541.2818	386.7127	**377.4789**
Z500	132h	471.5472	631.6456	485.4492	608.7734	464.0384	**437.4839**
Z500	144h	566.6680	729.6151	595.1192	743.3179	569.2445	**542.7397**
Z500	156h	654.4902	822.9236	720.2494	832.6830	669.9283	**639.2373**
Z500	168h	747.2870	932.4173	830.2883	922.7379	754.8806	**747.1750**
Z500	180h	868.6595	1015.7405	923.0644	963.3164	**815.4693**	898.6278
Z500	192h	979.1869	1095.5909	1031.9875	1014.1516	**859.9232**	1023.4053
Z500	204h	1044.4335	1171.7235	1098.2249	1110.0590	**898.6318**	1120.0131
Z500	216h	1110.4524	1237.9779	1173.1740	1239.1351	**958.4204**	1156.8152
Z500	228h	1212.0978	1314.9546	1266.0661	1261.9217	**1005.6409**	1239.9979
Z500	240h	1273.6925	1367.5504	1354.0935	1285.5398	**1044.5271**	1315.3407

18

Table 3: Greatest absolute difference in per-strata RMSE for global subregion. Lower is more fair; most fair for each variable and lead time is bolded.

Variable	Lead time (h)	Model					
		GraphCast	Keisler	Pangu-Weather	Spherical CNN	FuXi	NeuralGCM
T850	12h	**0.2525**	0.5555	0.3504	0.4085	0.2690	0.2599
T850	24h	**0.2852**	0.5617	0.3779	0.4630	0.2981	0.3243
T850	36h	**0.3363**	0.6454	0.4780	0.5130	0.3512	0.3723
T850	48h	**0.3880**	0.6931	0.5075	0.5734	0.4074	0.4177
T850	60h	**0.4623**	0.7767	0.5796	0.6264	0.4834	0.4862
T850	72h	**0.5562**	0.8714	0.6702	0.8082	0.5863	0.5778
T850	84h	0.6994	1.0025	0.7491	0.9256	0.7134	**0.6865**
T850	96h	0.8757	1.1339	0.9501	1.1201	0.9017	**0.8381**
T850	108h	1.0833	1.3553	1.1729	1.3028	1.1138	**1.0592**
T850	120h	1.3296	1.6098	1.4336	1.5700	1.3764	**1.3057**
T850	132h	1.6137	1.8671	1.6829	1.7964	**1.5735**	1.5992
T850	144h	1.9168	2.1653	1.9563	2.1541	**1.8085**	1.9220
T850	156h	2.2034	2.5199	2.2203	2.3437	**2.0344**	2.2378
T850	168h	2.4912	2.8395	2.5085	2.8486	**2.2963**	2.5705
T850	180h	2.7716	3.1276	2.7775	3.0715	**2.5446**	2.8682
T850	192h	3.0267	3.4037	3.1109	3.4501	**2.7923**	3.1401
T850	204h	3.2891	3.6766	3.3345	3.5138	**3.0081**	3.4233
T850	216h	3.5752	3.9070	3.6220	3.7692	**3.1939**	3.6968
T850	228h	3.8532	4.1115	3.7643	3.8652	**3.3680**	3.9615
T850	240h	4.0787	4.3223	4.0785	4.2605	**3.5287**	4.1710
Z500	12h	10.4583	22.0202	**7.0142**	13.0860	9.6233	12.3408
Z500	24h	15.2147	23.3950	15.3775	29.7619	14.1225	**13.2607**
Z500	36h	31.6671	47.2062	35.2885	52.6038	30.2638	**27.0468**
Z500	48h	55.0884	79.2753	56.8891	87.0013	53.2712	**50.2599**
Z500	60h	84.5594	118.5651	89.9188	120.1655	81.1725	**77.4975**
Z500	72h	119.6162	165.2460	124.3231	161.8944	114.0495	**113.2731**
Z500	84h	159.4383	218.3120	169.9461	206.6974	**154.0163**	156.4037
Z500	96h	206.9141	276.7293	217.2961	265.7229	**201.8156**	203.6802
Z500	108h	265.2308	340.8177	278.5598	324.6950	**254.1852**	257.5620
Z500	120h	330.6048	409.0917	342.7813	394.7158	**315.9001**	320.4175
Z500	132h	398.4901	481.7423	408.0717	477.3002	**374.1447**	375.0295
Z500	144h	472.8915	560.7308	480.2798	572.4723	**442.6990**	445.9015
Z500	156h	553.3959	647.4817	560.9786	652.9538	**519.2081**	530.1986
Z500	168h	635.8493	731.0427	640.5657	732.2401	**589.3926**	609.7468
Z500	180h	705.7083	800.0373	720.1483	795.3998	**644.0070**	698.6875
Z500	192h	769.0193	861.8439	789.5368	880.8382	**684.0959**	791.0014
Z500	204h	833.2273	928.2371	863.7943	947.5966	**722.9894**	882.7328
Z500	216h	900.5285	993.3099	932.0408	1031.0736	**765.0671**	953.4226
Z500	228h	968.6828	1051.8553	1003.9197	1105.4598	**802.7399**	1011.1210
Z500	240h	1025.1756	1104.4001	1060.0999	1155.7330	**833.8870**	1066.3462

Table 4: Greatest absolute difference in per-strata RMSE for income. Lower is more fair; most fair for each variable and lead time is bolded.

Variable	Lead time (h)	Model					
		GraphCast	Keisler	Pangu-Weather	Spherical CNN	FuXi	NeuralGCM
T850	12h	0.0620	0.0825	0.0751	0.0774	0.0642	**0.0542**
T850	24h	0.0754	0.1048	**0.0727**	0.1140	0.0797	0.0805
T850	36h	**0.0715**	0.1201	0.0813	0.0972	0.0757	0.0758
T850	48h	0.0937	0.1607	0.1106	0.1952	0.0928	**0.0754**
T850	60h	0.1423	0.2117	0.1430	0.2091	0.1405	**0.1181**
T850	72h	0.2078	0.2854	0.2241	0.3468	0.2050	**0.1791**
T850	84h	0.2900	0.3773	0.2926	0.4009	0.2881	**0.2559**
T850	96h	0.3875	0.4873	0.4117	0.6024	0.3822	**0.3522**
T850	108h	0.5282	0.6422	0.5619	0.6514	0.5243	**0.4859**
T850	120h	0.6864	0.8056	0.7235	0.8795	0.6860	**0.6450**
T850	132h	0.8621	0.9584	0.8995	0.9707	**0.8004**	0.8119
T850	144h	1.0326	1.1233	1.0585	1.1959	**0.9227**	0.9777
T850	156h	1.2090	1.2809	1.2427	1.3127	**1.0478**	1.1458
T850	168h	1.3726	1.4249	1.4092	1.5043	**1.1584**	1.3107
T850	180h	1.5107	1.5502	1.5566	1.6087	**1.2506**	1.4676
T850	192h	1.6483	1.6787	1.6764	1.7082	**1.3365**	1.6183
T850	204h	1.7905	1.7966	1.7819	1.8130	**1.4103**	1.7575
T850	216h	1.9016	1.9114	1.8654	1.9200	**1.4795**	1.8932
T850	228h	1.9866	2.0008	1.9558	2.0456	**1.5437**	1.9994
T850	240h	2.0647	2.0616	1.9952	2.1247	**1.5983**	2.0702
Z500	12h	**0.8108**	3.6642	1.6727	5.9048	1.5137	1.6957
Z500	24h	7.2642	8.9651	8.9447	13.8836	7.8770	**5.0367**
Z500	36h	18.9145	19.0145	20.9362	34.6394	18.7908	**15.1110**
Z500	48h	34.0168	34.0692	37.4726	51.7026	33.1263	**28.8815**
Z500	60h	52.3629	53.6224	56.2572	77.0541	50.8687	**46.4533**
Z500	72h	74.6146	84.2772	80.9830	104.9152	73.3257	**68.6393**
Z500	84h	100.2624	118.3149	108.8336	134.4815	100.0320	**95.4571**
Z500	96h	129.4711	156.8515	140.8503	167.4550	130.5978	**124.9093**
Z500	108h	163.7621	196.7506	176.3627	207.2879	165.2451	**159.4563**
Z500	120h	201.4575	237.4061	215.1524	247.2022	202.5977	**196.7490**
Z500	132h	240.7642	279.0208	257.4120	292.4811	**236.1156**	236.5664
Z500	144h	282.1859	323.2796	301.8338	331.7819	**269.7027**	277.7673
Z500	156h	325.4654	367.9642	347.4286	370.2875	**304.1304**	323.0253
Z500	168h	366.2331	413.1306	392.5974	414.4043	**337.6676**	365.8929
Z500	180h	404.1501	454.5309	436.6129	460.6266	**368.8637**	410.7149
Z500	192h	441.7336	493.7207	476.3061	490.5075	**397.4898**	457.3617
Z500	204h	481.4574	531.8207	516.7449	532.7525	**424.5340**	503.4393
Z500	216h	517.2955	566.0298	550.1209	568.5136	**448.0975**	543.1820
Z500	228h	550.2756	594.4706	579.6324	602.9630	**467.4228**	576.0455
Z500	240h	577.7541	619.7738	600.2285	620.6610	**483.7225**	606.3814

20

Table 5: Greatest absolute difference in per-strata RMSE for landcover. Lower is more fair; most fair for each variable and lead time is bolded.

Variable	Lead time (h)	Model					
		GraphCast	Keisler	Pangu-Weather	Spherical CNN	FuXi	NeuralGCM
T850	12h	0.0119	0.0022	0.0047	**0.0014**	0.0305	0.0301
T850	24h	0.0518	0.0262	0.0542	0.0331	0.0662	**0.0211**
T850	36h	0.0744	**0.0258**	0.0703	0.0454	0.0855	0.0497
T850	48h	0.0897	**0.0398**	0.0831	0.0640	0.1020	0.0756
T850	60h	0.0988	**0.0456**	0.1042	0.0762	0.1130	0.0922
T850	72h	0.1061	**0.0546**	0.1077	0.0942	0.1215	0.1076
T850	84h	0.1089	**0.0554**	0.1296	0.1037	0.1271	0.1156
T850	96h	0.1090	**0.0555**	0.1206	0.1090	0.1308	0.1196
T850	108h	0.1045	**0.0497**	0.1313	0.1099	0.1266	0.1158
T850	120h	0.0925	**0.0389**	0.1132	0.1083	0.1189	0.1059
T850	132h	0.0718	**0.0263**	0.1144	0.1036	0.0845	0.0873
T850	144h	0.0500	**0.0140**	0.0865	0.0825	0.0631	0.0705
T850	156h	0.0254	**0.0024**	0.0791	0.0762	0.0415	0.0541
T850	168h	**0.0014**	0.0160	0.0446	0.0560	0.0190	0.0376
T850	180h	0.0253	0.0335	0.0475	0.0439	**0.0007**	0.0155
T850	192h	0.0465	0.0549	0.0235	0.0201	0.0139	**0.0059**
T850	204h	0.0663	0.0833	0.0392	**0.0147**	0.0206	0.0219
T850	216h	0.0814	0.1052	0.0195	**0.0062**	0.0259	0.0327
T850	228h	0.1004	0.1206	0.0256	**0.0227**	0.0328	0.0507
T850	240h	0.1243	0.1318	**0.0039**	0.0478	0.0423	0.0659
Z500	12h	1.1498	4.0162	**0.9773**	2.4792	1.6285	1.8373
Z500	24h	**2.5139**	5.8507	2.7293	5.1420	3.3727	2.9665
Z500	36h	**5.1433**	8.9834	5.8332	9.6810	6.1696	5.7374
Z500	48h	**9.4250**	13.8543	10.1021	14.7946	10.4900	9.5702
Z500	60h	14.8999	20.7261	16.1918	21.7804	16.0543	**14.4554**
Z500	72h	21.4036	28.3228	22.4379	28.5432	22.7172	**20.1387**
Z500	84h	28.8944	36.0126	29.9796	37.6959	30.2328	**27.1628**
Z500	96h	37.2341	44.2808	37.3130	46.6026	38.5729	**34.4391**
Z500	108h	45.4507	53.2869	45.8862	57.6306	47.2646	**41.9945**
Z500	120h	53.2044	63.1831	55.7587	68.9327	56.2924	**49.9061**
Z500	132h	61.3276	73.3235	66.3274	80.2869	63.5645	**58.8711**
Z500	144h	69.6294	82.5196	76.2810	92.0807	72.1485	**68.2075**
Z500	156h	77.3385	91.0754	86.4044	104.6094	80.2376	**77.3269**
Z500	168h	**85.9806**	100.1707	97.3472	115.3360	87.0638	88.4507
Z500	180h	96.4382	109.5743	110.5671	127.2699	**94.6042**	100.2435
Z500	192h	107.7786	118.8574	123.4246	137.6266	**104.2935**	110.5522
Z500	204h	118.3307	127.7590	137.4269	151.7028	**114.9430**	121.0782
Z500	216h	126.9011	137.7304	148.8532	163.5775	**124.9670**	131.9841
Z500	228h	**133.3081**	146.0886	161.5919	176.7622	133.9938	142.6224
Z500	240h	**139.7696**	152.9192	172.9741	186.9395	142.3599	153.2736

21

Table 6: Variance of per-strata RMSE for territory. Lower is more fair; most fair for each variable and lead time is bolded.

Variable	Lead time (h)	Model					
		GraphCast	Keisler	Pangu-Weather	Spherical CNN	FuXi	NeuralGCM
T850	12h	0.0059	0.0239	0.0092	0.0165	**0.0058**	0.0076
T850	24h	**0.0096**	0.0279	0.0121	0.0168	0.0097	0.0107
T850	36h	**0.0135**	0.0382	0.0186	0.0307	0.0138	0.0142
T850	48h	**0.0178**	0.0466	0.0221	0.0323	0.0184	0.0183
T850	60h	0.0251	0.0620	0.0299	0.0547	0.0255	**0.0251**
T850	72h	0.0373	0.0835	0.0443	0.0716	0.0372	**0.0356**
T850	84h	0.0573	0.1176	0.0607	0.1101	0.0561	**0.0524**
T850	96h	0.0893	0.1698	0.0994	0.1556	0.0876	**0.0795**
T850	108h	0.1375	0.2443	0.1423	0.2218	0.1364	**0.1235**
T850	120h	0.2059	0.3395	0.2291	0.3035	0.2074	**0.1919**
T850	132h	0.2959	0.4561	0.3103	0.4021	**0.2714**	0.2779
T850	144h	0.4186	0.5987	0.4553	0.5464	**0.3716**	0.3909
T850	156h	0.5656	0.7738	0.5670	0.7006	**0.4904**	0.5290
T850	168h	0.7351	0.9761	0.7595	0.9217	**0.6140**	0.6940
T850	180h	0.9111	1.1959	0.9136	1.1105	**0.7442**	0.8872
T850	192h	1.1169	1.4065	1.1541	1.3722	**0.8763**	1.0970
T850	204h	1.3242	1.6228	1.3345	1.5895	**1.0046**	1.3022
T850	216h	1.5543	1.8264	1.5862	1.8438	**1.1379**	1.5319
T850	228h	1.7904	2.0273	1.7694	2.0041	**1.2647**	1.7675
T850	240h	2.0216	2.2219	2.0619	2.2228	**1.3857**	1.9841
Z500	12h	6.1246	19.7576	6.5390	26.6958	**5.4692**	8.3412
Z500	24h	32.5049	83.0658	35.6558	119.9938	27.7501	**19.6303**
Z500	36h	143.1572	279.3724	140.8770	373.2934	120.7857	**93.2486**
Z500	48h	422.6683	763.1224	392.4690	853.2862	369.6252	**299.1150**
Z500	60h	987.4937	1701.4127	949.6804	1737.7194	876.4381	**762.7267**
Z500	72h	1922.5214	3308.0522	1841.8360	3359.2755	1730.4532	**1597.9239**
Z500	84h	3460.4605	5910.8440	3581.2083	5685.9188	3114.8778	**3035.5692**
Z500	96h	5878.2943	9701.7932	5924.0644	9238.9938	5365.4816	**5199.0114**
Z500	108h	9207.0815	14545.4886	9712.0473	14644.0367	8691.7610	**8420.0934**
Z500	120h	13458.0770	20514.0618	14100.7981	20498.3937	13073.7371	**12613.6073**
Z500	132h	19099.0530	28397.0361	20510.6848	27854.1528	18151.6719	**17898.7947**
Z500	144h	26886.4435	38804.6110	27905.5223	38417.8133	**24577.2698**	24711.4568
Z500	156h	36642.9245	51445.5371	38171.4196	51472.3563	**32413.7343**	33955.2442
Z500	168h	48409.7383	65480.8310	48605.6695	66563.1440	**41054.8529**	45401.1447
Z500	180h	60518.6516	80059.5577	62042.4154	82184.3559	**49440.1657**	58908.7073
Z500	192h	72613.8939	93940.8663	74645.1235	94987.2438	**56671.8077**	74045.3921
Z500	204h	85533.4150	108180.5635	89582.7398	107801.6592	**63250.6773**	90607.4881
Z500	216h	100214.9498	122220.9953	103077.6203	118576.9672	**69991.3504**	106317.4791
Z500	228h	116333.6458	137609.8284	120685.8377	131908.1464	**76345.2022**	122233.5907
Z500	240h	131597.0478	153879.3978	135534.6276	143461.2929	**82097.1713**	137038.3218

22

Table 7: Variance of per-strata RMSE for global subregion. Lower is more fair; most fair for each variable and lead time is bolded. Smallest value determined before rounding to fourth decimal digit for display.

Variable	Lead time (h)	Model					
		GraphCast	Keisler	Pangu-Weather	Spherical CNN	FuXi	NeuralGCM
T850	12h	**0.0040**	0.0191	0.0074	0.0108	0.0040	0.0054
T850	24h	**0.0058**	0.0195	0.0083	0.0128	0.0058	0.0073
T850	36h	0.0076	0.0266	0.0123	0.0170	**0.0075**	0.0093
T850	48h	0.0099	0.0321	0.0142	0.0237	**0.0096**	0.0112
T850	60h	0.0147	0.0432	0.0184	0.0326	**0.0140**	0.0150
T850	72h	0.0240	0.0603	0.0297	0.0528	0.0226	**0.0225**
T850	84h	0.0400	0.0885	0.0417	0.0735	0.0377	**0.0355**
T850	96h	0.0654	0.1291	0.0742	0.1152	0.0627	**0.0577**
T850	108h	0.1031	0.1828	0.1060	0.1500	0.0997	**0.0917**
T850	120h	0.1575	0.2533	0.1753	0.2296	0.1554	**0.1441**
T850	132h	0.2307	0.3424	0.2346	0.2908	**0.2041**	0.2146
T850	144h	0.3239	0.4540	0.3420	0.4245	**0.2741**	0.3044
T850	156h	0.4354	0.5892	0.4239	0.5038	**0.3547**	0.4125
T850	168h	0.5633	0.7316	0.5709	0.6931	**0.4451**	0.5456
T850	180h	0.7000	0.8827	0.6815	0.8021	**0.5407**	0.6897
T850	192h	0.8463	1.0458	0.8625	1.0085	**0.6392**	0.8390
T850	204h	0.9986	1.2096	0.9686	1.0821	**0.7371**	0.9964
T850	216h	1.1588	1.3546	1.1507	1.2710	**0.8334**	1.1658
T850	228h	1.3176	1.4905	1.2595	1.3367	**0.9237**	1.3212
T850	240h	1.4755	1.6207	1.4524	1.5565	**1.0082**	1.4636
Z500	12h	4.3923	21.0451	**2.8972**	13.7473	4.1863	7.5274
Z500	24h	20.3463	51.3661	23.1773	69.7545	16.2691	**11.0202**
Z500	36h	100.9786	180.1252	103.6128	257.4925	81.9689	**58.8206**
Z500	48h	306.4674	508.7010	311.7182	654.5374	260.7049	**211.2787**
Z500	60h	716.7357	1184.5767	745.8135	1328.9283	627.4897	**550.1721**
Z500	72h	1409.4286	2363.1666	1476.1021	2530.5781	1266.1543	**1185.5958**
Z500	84h	2530.5646	4270.6684	2772.6681	4229.7121	2300.8085	**2260.5735**
Z500	96h	4226.6600	7043.0612	4561.6586	6801.1818	3926.2459	**3892.6980**
Z500	108h	6720.7189	10643.8530	7468.2495	10438.1276	6378.4510	**6359.9607**
Z500	120h	10141.6595	15290.3272	10987.4233	15390.8119	**9782.2574**	9793.6826
Z500	132h	14620.2634	21372.4804	15893.7948	21336.5717	**13540.9848**	14039.6015
Z500	144h	20488.9905	29376.4397	21538.2609	28923.9358	**18291.9364**	19539.8322
Z500	156h	27792.6869	39121.5091	29073.4592	38107.4375	**24161.9448**	26805.0344
Z500	168h	36070.0516	49415.4562	37029.6547	49476.3792	**30594.7232**	35135.2208
Z500	180h	44563.2319	59680.5409	46715.6210	59530.9165	**36729.6627**	44896.8645
Z500	192h	53264.2736	69510.8777	55549.5099	69291.2225	**42029.8539**	56232.0981
Z500	204h	62941.2933	80014.6105	65986.8602	78463.7736	**47054.4341**	69073.4405
Z500	216h	73576.4355	90367.1381	76461.9376	88426.2503	**52021.9554**	81403.3079
Z500	228h	84684.8208	101170.3770	88451.4026	99330.6919	**56592.5334**	92347.6782
Z500	240h	95626.2297	111864.2591	98694.2737	109405.8148	**60587.5795**	102322.9160

Table 8: Variance of per-strata RMSE for income. Lower is more fair; most fair for each variable and lead time is bolded. Smallest value determined before rounding to fourth decimal digit for display.

Variable	Lead time (h)	Model					
		GraphCast	Keisler	Pangu-Weather	Spherical CNN	FuXi	NeuralGCM
T850	12h	0.0006	0.0013	0.0009	0.0011	0.0007	**0.0006**
T850	24h	0.0010	0.0016	0.0011	0.0017	0.0011	**0.0009**
T850	36h	0.0011	0.0019	0.0013	0.0016	0.0012	**0.0010**
T850	48h	0.0013	0.0033	0.0016	0.0056	0.0014	**0.0010**
T850	60h	0.0026	0.0061	0.0026	0.0057	0.0025	**0.0018**
T850	72h	0.0062	0.0125	0.0073	0.0212	0.0059	**0.0044**
T850	84h	0.0139	0.0243	0.0145	0.0273	0.0135	**0.0106**
T850	96h	0.0276	0.0438	0.0312	0.0603	0.0265	**0.0227**
T850	108h	0.0488	0.0724	0.0543	0.0721	0.0478	**0.0426**
T850	120h	0.0798	0.1103	0.0893	0.1264	0.0785	**0.0716**
T850	132h	0.1238	0.1542	0.1313	0.1532	**0.1045**	0.1113
T850	144h	0.1762	0.2094	0.1835	0.2357	**0.1380**	0.1600
T850	156h	0.2393	0.2702	0.2485	0.2810	**0.1782**	0.2193
T850	168h	0.3072	0.3337	0.3235	0.3675	**0.2187**	0.2877
T850	180h	0.3717	0.3958	0.3883	0.4064	**0.2567**	0.3626
T850	192h	0.4403	0.4646	0.4587	0.4712	**0.2931**	0.4383
T850	204h	0.5147	0.5308	0.5126	0.5191	**0.3260**	0.5095
T850	216h	0.5801	0.5981	0.5677	0.5882	**0.3587**	0.5835
T850	228h	0.6361	0.6526	0.6199	0.6570	**0.3897**	0.6473
T850	240h	0.6864	0.6947	0.6519	0.7183	**0.4179**	0.6952
Z500	12h	**0.1028**	2.0068	0.4295	4.7712	0.3603	0.6834
Z500	24h	8.1396	11.1313	11.5812	32.1529	9.3156	**3.6432**
Z500	36h	58.2438	50.2198	68.4765	189.2996	56.8211	**36.4330**
Z500	48h	189.4209	184.8858	223.4966	442.7660	179.4246	**136.8048**
Z500	60h	451.0046	520.4977	519.4968	974.0071	428.2830	**358.7665**
Z500	72h	911.0966	1229.6501	1080.3229	1821.1763	883.6421	**785.7836**
Z500	84h	1646.9627	2382.9868	1968.3536	2952.4151	1629.0901	**1513.8882**
Z500	96h	2737.5665	4144.1104	3276.2421	4528.4890	2747.9434	**2587.6919**
Z500	108h	4348.0463	6467.1286	5135.8483	6914.8034	4382.9351	**4201.6065**
Z500	120h	6597.2991	9373.6499	7560.5792	9862.9344	6573.8777	**6412.9097**
Z500	132h	9533.7548	12964.9450	10791.6058	13911.4043	**8959.9675**	9339.7532
Z500	144h	13148.0557	17427.2140	14753.4857	18254.7028	**11740.4081**	12892.9825
Z500	156h	17445.2287	22671.1704	19650.6572	22708.4878	**14994.6352**	17418.3039
Z500	168h	22182.4991	28490.4680	25084.7184	28230.3578	**18601.2094**	22431.9354
Z500	180h	27146.0603	34351.0365	31108.3918	34170.3147	**22273.9916**	28154.0990
Z500	192h	32239.4210	40199.3865	36779.7222	38994.5403	**25839.6953**	34533.8555
Z500	204h	37995.0056	46201.5532	42988.3711	45546.9357	**29384.0512**	41433.0906
Z500	216h	43861.1521	52094.4753	48642.4069	51911.1326	**32665.9497**	48114.7002
Z500	228h	49661.7138	57430.4755	54233.6775	58344.7264	**35546.9475**	54187.6957
Z500	240h	54749.8350	62421.6302	58373.7147	63053.7066	**38117.6736**	60038.5224

Table 9: Variance of per-strata RMSE for landcover. Lower is more fair; most fair for each variable and lead time is bolded. Smallest value determined before rounding to fourth decimal digit for display.

Variable	Lead time (h)	Model					
		GraphCast	Keisler	Pangu-Weather	Spherical CNN	FuXi	NeuralGCM
T850	12h	0.0000	0.0000	0.0000	**0.0000**	0.0002	0.0002
T850	24h	0.0007	0.0002	0.0007	0.0003	0.0011	**0.0001**
T850	36h	0.0014	**0.0002**	0.0012	0.0005	0.0018	0.0006
T850	48h	0.0020	**0.0004**	0.0017	0.0010	0.0026	0.0014
T850	60h	0.0024	**0.0005**	0.0027	0.0015	0.0032	0.0021
T850	72h	0.0028	**0.0007**	0.0029	0.0022	0.0037	0.0029
T850	84h	0.0030	**0.0008**	0.0042	0.0027	0.0040	0.0033
T850	96h	0.0030	**0.0008**	0.0036	0.0030	0.0043	0.0036
T850	108h	0.0027	**0.0006**	0.0043	0.0030	0.0040	0.0034
T850	120h	0.0021	**0.0004**	0.0032	0.0029	0.0035	0.0028
T850	132h	0.0013	**0.0002**	0.0033	0.0027	0.0018	0.0019
T850	144h	0.0006	**0.0000**	0.0019	0.0017	0.0010	0.0012
T850	156h	0.0002	**0.0000**	0.0016	0.0014	0.0004	0.0007
T850	168h	**0.0000**	0.0001	0.0005	0.0008	0.0001	0.0004
T850	180h	0.0002	0.0003	0.0006	0.0005	**0.0000**	0.0001
T850	192h	0.0005	0.0008	0.0001	0.0001	0.0000	**0.0000**
T850	204h	0.0011	0.0017	0.0004	**0.0001**	0.0001	0.0001
T850	216h	0.0017	0.0028	0.0001	**0.0000**	0.0002	0.0003
T850	228h	0.0025	0.0036	0.0002	**0.0001**	0.0003	0.0006
T850	240h	0.0039	0.0043	**0.0000**	0.0006	0.0004	0.0011
Z500	12h	0.3305	4.0325	**0.2388**	1.5367	0.6630	0.8439
Z500	24h	**1.5799**	8.5578	1.8622	6.6101	2.8439	2.2000
Z500	36h	**6.6135**	20.1753	8.5065	23.4304	9.5159	8.2295
Z500	48h	**22.2078**	47.9855	25.5133	54.7201	27.5102	22.8971
Z500	60h	55.5015	107.3930	65.5437	118.5960	64.4349	**52.2397**
Z500	72h	114.5290	200.5459	125.8643	203.6786	129.0179	**101.3914**
Z500	84h	208.7222	324.2265	224.6944	355.2449	228.5063	**184.4539**
Z500	96h	346.5953	490.1982	348.0649	542.9503	371.9671	**296.5129**
Z500	108h	516.4417	709.8745	526.3853	830.3223	558.4856	**440.8835**
Z500	120h	707.6771	998.0250	777.2581	1187.9308	792.2084	**622.6550**
Z500	132h	940.2671	1344.0848	1099.8318	1611.4985	1010.1114	**866.4512**
Z500	144h	1212.0642	1702.3716	1454.6969	2119.7129	1301.3511	**1163.0654**
Z500	156h	1495.3124	2073.6823	1866.4296	2735.7801	1609.5192	**1494.8609**
Z500	168h	**1848.1638**	2508.5428	2369.1183	3325.6011	1895.0281	1955.8816
Z500	180h	2325.0811	3001.6319	3056.2699	4049.4052	**2237.4910**	2512.1880
Z500	192h	2904.0572	3531.7694	3808.4100	4735.2684	**2719.2835**	3055.4490
Z500	204h	3500.5399	4080.5920	4721.5363	5753.4311	**3302.9746**	3664.9805
Z500	216h	4025.9693	4742.4189	5539.3190	6689.3969	**3904.1884**	4354.9488
Z500	228h	**4442.7599**	5335.4729	6527.9828	7811.2172	4488.5863	5085.2891
Z500	240h	**4883.8882**	5846.0681	7480.0098	8736.5929	5066.5870	5873.1976

E GENERAL FAIRNESS EXPERIMENTS ON ADDITIONAL VARIABLES

We repeat the general fairness experiments from section 4 for precipitation (6hr and 24hr cumulative), 2m temperature, and wind speed (U and V components at 10m). Forecast data on these variables was not available for every model for WB2. We report results on each variable for the models where it was available. These experiments find generally the same results as those on T850 and Z500: systemic bias in model performance across models that increases with lead time.

E.1 PRECIPITATION

General fairness. We look at total precipitation over 6 hour (P6) and 24 hour (P24) periods for GraphCast and FuXi. Greatest absolute difference (Figure 9) and variance (Figure 10) in RMSE are plotted. Except on the landcover attribute at high lead times, GraphCast is more fair than Fuxi. It is interesting that GraphCast is generally fairer than FuXi at high lead times, as FuXi outperforms GraphCast on traditional, globally-averaged performance in those cases (Figure 11).

E.2 2M TEMPERATURE AND WIND SPEED

General fairness. We look at air temperature at 2m (T2m) and wind speed at 10m (U10m and V10m) on GraphCast, Pangu-Weather, and FuXi, the only models that had data for these variables.
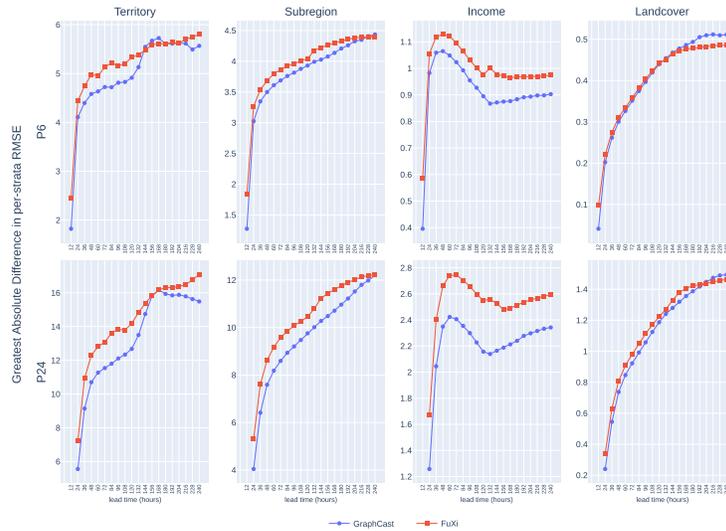
25

Figure 9: Greatest absolute difference of any two per-strata RMSE for each attribute when predicting precipitation for 6 hours (P6) and 24 hours (P24) at different lead times. Lower difference is more fair.
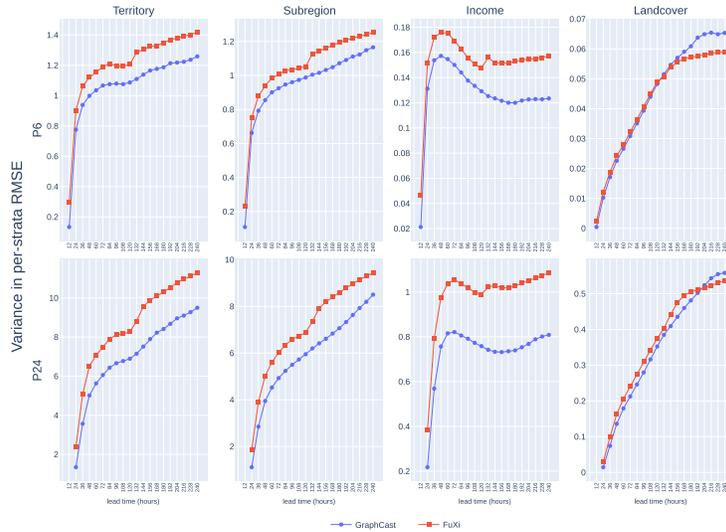

Figure 10: Variance in per-strata RMSE for each attribute when predicting precipitation for 6 hours (P6) and 24 hours (P24) at different lead times. Lower variance is more fair.
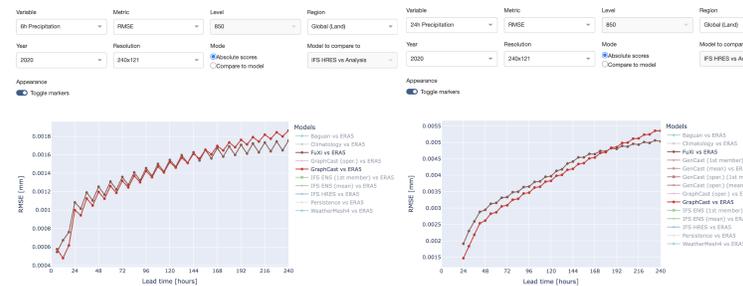

Figure 11: Performance of GraphCast and FuXi on P6 and P24 in terms of globally-averaged RMSE. Lower is better. Screenshot taken from Google's WeatherBench dashboard.
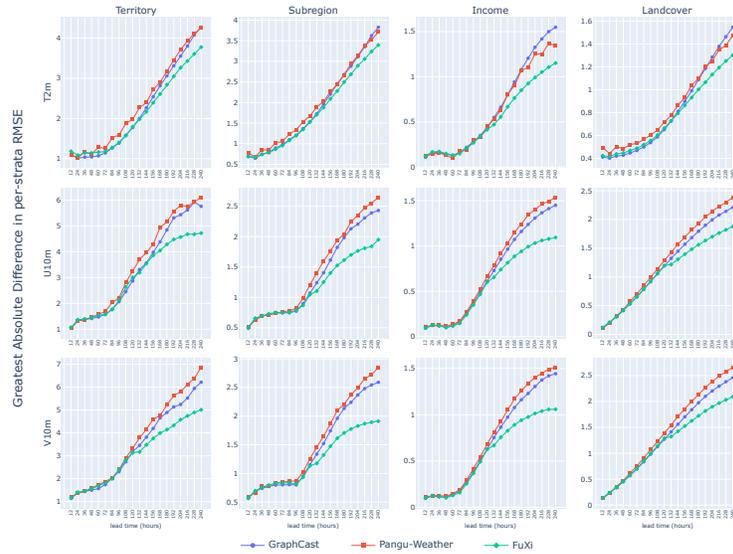
26

Figure 12: Greatest absolute difference of any two per-strata RMSE for each attribute on 2m temperature (T2m) and the U and V components of wind speed at 10m (U10m and V10m, respectively). Lower difference is more fair.
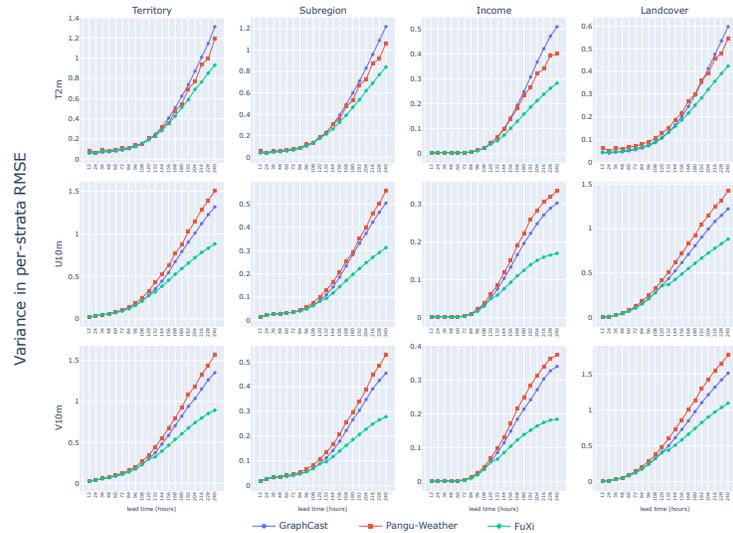

Figure 13: Variance in per-strata RMSE for each attribute on 2m temperature (T2m) and the U and V components of wind speed at 10m (U10m and V10m, respectively). Lower variance is more fair.

Greatest absolute difference (Figure 12) and variance (Figure 13) in RMSE are plotted. For high lead times, FuXi is generally the most fair. At low lead times on 2m temperature, GraphCast is the most fair—an interesting result as it becomes the least fair at high lead times. At low lead times on the wind speed variables, GraphCast and Pangu-Weather alternate being the most fair. At high lead times, Pangu-Weather is the least fair in predicting 10m wind speeds. As with every other variable assessed, unfairness and the inter-model disparities in unfairness grow as lead time grows.

F   SUPPLEMENTAL FIGURES

Figure 14 depicts the same results as the income attribute experiment in subsection 4.4 while zoomed in on low lead times. It is seen that at low lead times, all models perform worst in lower income countries.
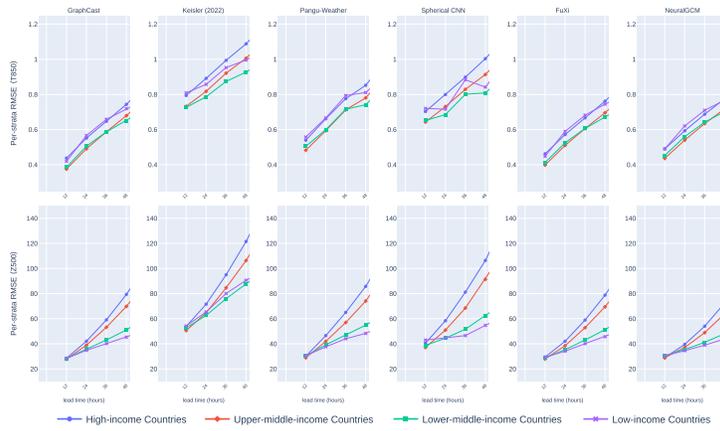

Figure 14: Per-strata RMSE for the income attribute of each model for the first 48 hours of lead time.